HHS Public Access

Author manuscript

Int J Pharm. Author manuscript; available in PMC 2024 January 12.

Published in final edited form as:

Int J Pharm. 2023 December 15; 648: 123565. doi:10.1016/j.ijpharm.2023.123565.

Fast time-resolved micro-CT imaging of pharmaceutical tablets: Insights into water uptake and disintegration

Shumaiya Ferdoush[a], **Sarah Bu Kzam**[a], **Pedro H.C. Martins**[a], **Jan Dewanckele**[c], **Marcial Gonzalez**[a,b,*]

[a]School of Mechanical Engineering, Purdue University, West Lafayette, IN 47907, USA

[b]Ray W. Herrick Laboratories, Purdue University, West Lafayette, IN 47907, USA

[c]TESCAN XRE, Ghent, Belgium

Abstract

We use dynamic micro-computed tomography (micro-CT) with a high temporal resolution to visualize water penetration through the porous network of immediate-release pharmaceutical solid tablets and characterize dynamic swelling and disintegration mechanisms. We process the micro-CT images using two theoretical scenarios that reflect different paths of pore structure evolution: a scenario where tablet porosity remains constant during the swelling process and a scenario where the tablet porosity progressively diminishes and eventually closes during the swelling process. We calculate the time evolution of the volume of water absorbed by the tablet and, specifically, absorbed by the excipients and the pore structure, as well as the formation and evolution of cracks. In turn, the three-dimensional disintegration pattern of the tablets is reconstructed. Restricting attention to the limiting scenario where tablet porosity is assumed fixed during the swelling process, we couple liquid penetration due to capillary pressure described by the Lucas–Washburn theory with the first-order swelling kinetics of the excipients to provide a physical interpretation of the experimental observations. We estimate model parameters that are in agreement with values reported in the literature, and we demonstrate that water penetration is dominated by intra-particle porosity rather than inter-particle porosity.

Keywords

Tablet porosity; Dynamic micro-CT; Water uptake; Swelling; Capillary flow

[*]Corresponding author at: School of Mechanical Engineering, Purdue University, West Lafayette, IN 47907, USA. marcial-gonzalez@purdue.edu (M. Gonzalez).

Declaration of competing interest

The authors declare that they have no known competing financial interests or personal relationships that could have appeared to influence the work reported in this paper.

CRediT authorship contribution statement

Shumaiya Ferdoush: Methodology, Software, Validation, Formal analysis, Data curation, Writing – original draft, Visualization. **Sarah Bu Kzam:** Methodology, Software, Formal analysis. **Pedro H.C. Martins:** Conceptualization, Methodology, Investigation, Writing – review & editing. **Jan Dewanckele:** Conceptualization, Methodology, Investigation, Resources. **Marcial Gonzalez:** Conceptualization, Methodology, Resources, Writing – review & editing, Supervision, Project administration, Funding acquisition.

Appendix A. Supplementary data

Supplementary material related to this article can be found online at https://doi.org/10.1016/j.ijpharm.2023.123565.

1. Introduction

The most common orally administered solid unit dosage form for drug delivery is compacted tablets. The main advantages encompass accurate control of dosing, easy storage, cost-effectiveness, and easy administration. Tablet formulations generally consist of active pharmaceutical ingredients (APIs) and a mix of inactive ingredients, termed excipients, which must be physiologically inert (Desai et al., 2016). Excipients are critical to the tablet design, determining its functionality and performance. Controlling the release of API at the drug plasma level leads to reduced side effects while providing greater patient compliance and convenience (Abdul and Poddar, 2004). To achieve the desired release profile, one needs to have a well-researched view of API's fundamental physicochemical and biopharmaceutical properties, appropriate excipient selection, and manufacturing condition (Wen and Park, 2011). Different kinds of excipients, including disintegrants, fillers, binders, glidants, lubricants, antioxidants, ultraviolet absorbers, dissolution modifiers, absorbents, flavoring, agents, colorants, wetting agents, and preservatives may be added to the formulation (Kottke and Rudnic, 2002; Augsburger et al., 2007). For example, an excipient such as a soluble or insoluble filler (lactose/mannitol vs. microcrystalline cellulose) added to a formulation may affect the drug release rate in different ways (Rosiaux et al., 2014).

Different complex physical and chemical phenomena induce drug release from a pharmaceutical system, and a mathematical model to describe these mechanisms is difficult to find (Costa and Lobo, 2001). According to Siepmann and Peppas (2012), in many cases, simple empirical and semi-empirical models are sufficient to understand drug release mechanisms and design a new product. For example, Ferdoush and Gonzalez (2023) developed semi-mechanistic models to predict changes in dissolution profiles due to manufacturing process disturbances and studied how these models can enable real-time release testing. However, detailed information and complex mechanistic theories must be applied in many cases. According to Peppas and Narasimhan (2014), models that capture the mechanistic theory will provide new insights into the release mechanism when combined with precise experimental observations. Thus, realizing that the underlying coupled mechanics of imbibition, swelling, disintegration, and dissolution are still an open question. Specifically, the following dominant mechanisms of disintegration are identified (Quodbach and Kleinebudde, 2016; Markl and Zeitler, 2017; Faroongsarng and Peck, 1994; Moreton, 2008; Desai et al., 2016): (i) liquid intake through the open porous network by capillarity action, (ii) liquid transport from/to the pore-space network to/from the particles, (iii) liquid transport from particle to particle facilitated by the contact interfaces and solid bridges created during the compaction process, (iv) swelling of the particles due to liquid penetration, (v) deformation of the granular structure to relax internal stresses created during swelling, (vi) softening of particles and solid bridges due to liquid uptake, and (vii) breakage of solid bridges due to excessive relaxation of internal stress and mechanical softening. Characterizing these processes at the microstructure level is challenging because one needs to visualize them from the inside out. Another challenge lies in identifying the time scale of these processes, as sample relaxation or other processes can happen in seconds to minutes. Time-resolved micro-computed tomography (micro-CT) or 4D CT, where time is

defined as the fourth dimension, is an excellent non-destructive technique to visualize these mechanisms (Boever et al., 2021).

During a time-lapse imaging process, a series of individual scans is taken over a specific experiment time period, often referred to as ‘interrupted 4D’ experiments. Conversely, dynamic tomography does not incorporate any delays between individual scans. Instead, an uninterrupted acquisition approach is adopted during the scan time interval of the entire process in examination (Dewanckele et al., 2020). Dynamic micro-CT is a powerful imaging technique that can provide high temporal resolution, improved contrast, reduced motion artifacts, and accurate 3D reconstruction where no crucial information is lost. These advantages make it ideal for studying rapid dynamic processes in materials science, biology, and engineering, among other fields. However, time-lapse micro-CT is still useful for studying slower dynamic processes and changes that occur gradually and consistently over longer time scales (Hunter and Dewanckele, 2021; Dewanckele et al., 2021; van der Wal, 2021) such as corrosion of metals, creep processes, or slow crystallization phenomena (Boever et al., 2021). TESCAN, a leading global producer and supplier of scanning electron microscopes, has designed and manufactured the first dynamic micro-CT system to offer both sub-micron spatial resolution and high temporal resolution in a single system (Vacuum, 2022). Specifically, the TESCAN UniTOM HR’s high-resolution imaging capabilities make it a valuable tool for material characterization and failure analysis (Joseph et al., 2023; Pinto et al., 2023; Mesquita et al., 2022; Butenegro et al., 2022; Javanshour et al., 2023). However, these 4D micro-CT capabilities have yet to be used to quantify fast structural changes in pharmaceutical solid tablets and understand disintegration behavior (cf., quantitative studies of total volume increase of tablets or individual grains Rudnic et al., 1982).

In this study, a TESCAN UniTOM HR is used to visualize (i) penetration of water inside the tablet through the porous network and (ii) disintegration dynamics of immediate-release tablets, i.e., tablets that disintegrate and completely dissolve upon exposure to water in a few minutes (see, e.g., Markl and Zeitler (2017)). This rapid disintegration poses challenges for slower, time-lapse, or interrupted micro-CT procedures since water uptake, swelling, and disintegration processes cannot be paused during the experiment. We have also investigated the pore structure changes and estimated the time evolution of total tablet volume during swelling. Furthermore, we will provide a physical interpretation of the results obtained from these micro-CT images by identifying the water pathways as it fills the pore structure and it is absorbed by the swelling excipients (Hamraoui and Nylander, 2002; Washburn, 1921; Schott, 1992a,b).

The paper is organized as follows. Section 2 discusses materials for fabricating the tablets used in this study and methods for obtaining the dynamic micro-CT images. Microstructure reconstruction and segmentation process are also described in the same section. The micro-CT image processing results are presented in Section 3. Physical interpretation of the results is provided in the same section. Concluding remarks are presented in Section 4.

2. Materials and methods

2.1. Materials

Tablets were fabricated using a 6 mm die and a flat punch in a Gamlen D-Series bench-top compactor simulator. Four different in-die relative densities ρ_{in-die} (0.8, 0.85, 0.9, and 0.95) were achieved by varying tablet thickness and using a target weight of $M = 153$ mg. Upon tablet ejection from the die, the out-of-die relative density and tablet porosity ϵ_0 (0.262, 0.227, 0.175, and 0.139) were calculated from the tablet volume, mass, and true density of the powder blend. The formulation consisted of 89% w/w microcrystalline cellulose (Avicel PH 200; DuPont Nutrition, US), 9% w/w acetaminophen (APAP; Mallinckrodt Pharmaceuticals, US), 1% w/w magnesium stearate (MgSt; Spectrum Chemical Mfg. Corp., New Brunswick, NJ, US), and 1% w/w colloidal silica dioxide (Cab-O-Sil; Cabot Corporation, IL, US). Microcrystalline cellulose is widely used in pharmaceutical products as a binder and disintegrant in oral tablets (Rowe et al., 2009). Acetaminophen helps relieve pain and reduces fever. Magnesium stearate is the most widely used lubricant in pharmaceutical solid products. Colloidal Silica Dioxide is used as an anti-caking agent, adsorbent, disintegrant, and glidant to facilitate powder flow during processing (Rowe et al., 2009). Cab-O-Sil and MgSt can coat the particles, modify their wettability, and, thus, change the drug release rate of the compact (Rowe et al., 2009). The small amount of powder required for fabricating 40 tablets was premixed in a 20 ml glass vial.

2.2. Dynamic micro-CT imaging

To dynamically obtain the micro-CT scans of liquid penetration inside the tablets, the tablet was placed on a styrofoam sample holder with a syringe pump attached to inject water at a rate of 2 ml/min. The water was stained with CsCl for better contrast. Next, the in-situ setup was mounted on the rotation stage of the TESCAN UniTOM HR Fig. 1 shows the experimental setup and Fig. 2 shows a schematic of the TESCAN UniTOM HR and powered through the slip-ring of the system. By doing so, an endless, uninterrupted rotation of the complete setup was possible, as fluid cable tangling was prevented. As a result, the tablet absorbed water from the bottom through capillary uptake, which was continuously scanned.

A high temporal resolution was needed to capture the disintegration process's fast dynamics. The total time for complete wetting of the tablet was 7 mins. In the experiment, 100 uninterrupted tomograms at a temporal resolution of 4 s (200 projections/360°, 20 ms exposure time) per rotation could be obtained while the tablet absorbed water and swelled. The voxel size of the scan was 13 μm, small enough to visualize the deformation mechanics inside of the sample.

2.3. Microstructure reconstruction and segmentation

Time-resolved micro-CT images were processed using the software *Dragonfly* from Object Research Systems (Dragonfly 2022.1 [Computer software], 2022). Microstructure reconstruction and segmentation were realized following a multi-step process. Firstly, after cropping the images to reduce sources of outside noise, the range of attenuation values (i.e., densities) corresponding to the solid tablet throughout the experiment was identified. This range accounted for both dry and wet material, and it was different for tablets with different

initial relative densities or porosities. Next, the range of attenuation values (i.e., of densities) of the wet tablet was identified from the time-stamp at which the water absorption process reached steady-state conditions (i.e., the tablet is entirely wet). Table 1 shows the range of attenuation values for all four relative densities $\rho_{\text{in-die}}$. Lastly, at every time-stamp t recorded during the time-resolved micro-CT test, the total volume of the tablet V_{total} and the volume of the wet portion V_{wet} was computed using *Dragonfly*, the volume of the dry portion of the tablet follows from

$$V_{\text{total}}(t) = V_{\text{dry}}(t) + V_{\text{wet}}(t) \tag{1}$$

It is worth noting that the total volume of the tablet excludes the cracks formed during the water absorption process, which are resolved by the micro-CT scan. For consistency, the tablet's total volume and its wet portion were compared at the last time-stamp recorded and verified to be under 5% from each other for all four relative densities. This small inconsistency is adopted as the absolute error in estimating total tablet volume, which is then propagated throughout the calculations presented next in this section.

Various studies have been performed to understand microstructural changes within the wet portion of the tablet due to water penetration and swelling. Suzuki et al. (2022) studied water absorption inside orally disintegrating tablets using X-ray CT. Four formulations consisting of D-mannitol, microcrystalline cellulose, light anhydrous silicic acid, dextrin, aspartame, magnesium stearate, and donepezil hydrochloride were characterized. They observed that porous regions of voids up to 20 μm appeared inside the tablet after water absorption due to the break-up of bonds between particles and/or mannitol dissolving into the water. Schuchard and Berg (1991) studied the wicking of a composite of cellulose and superabsorbent carboxymethyl cellulose fiber networks, namely, two-dimensional fiber networks such as paper strips and three-dimensional fiber networks such as fluff pads. They observed that the inter-fiber pore network partially constricts due to fiber swelling. They quantified this change in morphology by a permeability factor, defined as the ratio of the swollen state wicking-equivalent radius to that in the unswollen state. Markl et al. (2017) developed models for liquid penetration in a swelling porous medium for micro-crystalline cellulose tablets by assuming that the rate of increase of the dry particles' volume is equal to the volumetric rate of liquid absorption by solid matrix. However, studies about the dynamic change of tablet microstructure and porosity due to water penetration inside the tablet are rarely found in the open literature. In the following study, the volume of water absorbed by the tablet V_{water} will be determined under the assumption that the swelling process is strictly additive in volume, that is, the volume of the wet and swollen excipient is equal to the volume of dry excipient plus the volume of water (Markl et al., 2017; Soundaranathan et al., 2020). The pore structure within the wet region is assumed to be occupied with water during absorption. Lastly, due to the lack of direct experimental evidence, the following two limiting scenarios for describing pore structure changes due to swelling are investigated:

1. Tablet porosity is fixed during the swelling process, as shown in Fig. 3(a).

2. Tablet porosity constricts with time during the swelling process and eventually closes at the infinite time or steady-state conditions, as shown in Fig. 3(b).

These two scenarios and the formation of cracks are discussed next in turn.

Tablet porosity is fixed during the swelling process.—The water inside the polymer $V_{\text{water}}^{\text{exc}}$ is then given by

$$V_{\text{water}}^{\text{exc}}(t) = [V_{\text{total}}(t) - V_{\text{total}}(0)][1 - \epsilon_0] \tag{2}$$

and the water inside the pore structure $V_{\text{water}}^{\text{void}}$ is given by

$$V_{\text{water}}^{\text{void}}(t) = \epsilon_0 V_{\text{wet}}(t) \tag{3}$$

Hence, the volume of water absorbed by the tablet is equal to

$$V_{\text{water}}(t) = [V_{\text{total}}(t) - V_{\text{total}}(0)][1 - \epsilon_0] + \epsilon_0 V_{\text{wet}}(t) \tag{4}$$

It is worth verifying that at $t = 0$, $V_{\text{water}}(0) = V_{\text{wet}}(0)\epsilon_0 = 0$, and noting that at $t \to \infty$, $V_{\text{total}}(\infty) = V_{\text{wet}}(\infty)$ and, thus, $V_{\text{water}}(\infty) = V_{\text{total}}(\infty) - V_{\text{total}}(0)(1 - \epsilon_0)$.

Tablet porosity constricts and closes during the swelling process.—Tablet porosity $\epsilon(t)$ depends on time and it is assumed to follow

$$\epsilon(t) = \epsilon_0 \left[1 - \frac{V_{\text{wet}}(t)}{V_{\text{total}}(t)}\right] \tag{5}$$

with $\epsilon(0) = \epsilon_0$ and $\epsilon(\infty) = 0$. Hence, incorporating the time dependency in Eq. (4), the volume of water absorbed by the tablet is equal to

$$V_{\text{water}}(t) = V_{\text{total}}(t)[1 - \epsilon(t)] - V_{\text{total}}(0)[1 - \epsilon(0)] + \epsilon(t)V_{\text{wet}}(t) \tag{6}$$

and, by using Eq. (5), it simplifies to

$$V_{\text{water}}(t) = [V_{\text{total}}(t) - V_{\text{total}}(0)][1 - \epsilon_0] + \epsilon_0 V_{\text{wet}}(t)\left[2 - \frac{V_{\text{wet}}(t)}{V_{\text{total}}(t)}\right] \tag{7}$$

It is worth noting that Eqs. (4) and (7) have the same limit at $t \to \infty$, that is $V_{water}(\infty) = V_{total}(\infty) - V_{total}(0)(1 - \epsilon_0)$. Furthermore, the water absorbed by the polymer is equal to

$$V_{water}^{exc}(t) = [V_{total}(t) - V_{total}(0)][1 - \epsilon_0] + \epsilon_0 V_{wet}(t) \tag{8}$$

and the water inside the pore space is equal to

$$V_{water}^{void}(t) = \epsilon(t) V_{wet}(t) = \epsilon_0 \left[1 - \frac{V_{wet}(t)}{V_{total}(t)}\right] V_{wet}(t) \tag{9}$$

Formation of cracks.—The volume of cracks formed during the water absorption process V_{cracks} is approximated using *Dragonfly* to estimate the volume of a cylinder that circumscribes the tablet V_{cyl}, and then from

$$V_{cyl}(t) = V_{total}(t) + V_{cracks}(t) \tag{10}$$

Due to software limitations, the circumscribed cylinder was manually adjusted to fit over the non-uniformly swollen tablet while attempting to strike a balance between overestimated and underestimated regions.

3. Results

The microstructure reconstruction and segmentation method described in Section 2.3 is followed to estimate the time evolution of total tablet volume. Fig. 4 shows that the total volume of the tablet at steady state conditions, that is, at a fully swollen state, increases with decreasing relative density. Furthermore, all tested tablets exhibit a period of time during which the rate of water uptake increases, as opposed to the otherwise decreasing trend in the rate of water uptake observed throughout the test, as shown in Fig. 5. For example, for the tablet with a relative density of 0.95, the rate of water uptake has a decreasing trend throughout the entire test except between 130 and 160 s. This change in curvature in the total tablet volume curve occurs when the tablet undergoes significant crack formation. Inserts in Fig. 4 show snapshots of tablet cross-sections at the beginning and the end of this non-monotonic region of the rate of water uptake. It is evident from the figures that (i) at the onset of this behavior, dry regions still exist within the tablet, and cracks are incipient, and (ii) at the end of this behavior, cracks are arrested, and most of the tablet is wet. The figures also indicate that with increasing relative density or decreasing tablet porosity, cracks form later and take longer to be arrested. Moreover, Figs. 6, 8, 10, and 12 show in greater detail the time evolution and two-dimensional morphology of crack formation and water absorption. In addition, Figs. 7, 9, 11, and 13 show in greater detail the time evolution and three-dimensional morphology of crack formation and water absorption. These figures are reconstructed from the time-resolved micro-CT images, and

they illustrate the three-dimensional disintegration pattern of the sample. As tablets absorb water, micro-cracks form in the wet region and propagate horizontally, i.e., on the plane perpendicular to water absorption and tablet compaction. The dry–wet interface is conical in shape, i.e., it propagates faster at the tablet boundaries. Figures indicate that larger cracks form towards the top of the tablet, where the conical interface eventually closes onto the top surface (see https://doi.org/10.1016/j.ijpharm.2023.123565supplemental material (water absorption videos)). It is known that the top corners and middle bottom half are denser than the top center and bottom corners of flat-faced tablets (see, e.g., Eiliazadeh et al. (2003)). This non-uniformity in porosity is due to frictional forces between the tooling and tablet during compaction. The plausible relationship between crack formation and the small non-uniformity in porosity can be elucidated by performing a high spatial resolution and time-consuming scan before conducting coarser but faster time-resolved imaging, if beyond the scope of this work.

Fig. 14 shows the time evolution of water volume absorbed inside the tablet for the two limiting scenarios considered here, namely (i) if tablet porosity is assumed fixed during the swelling process, i.e., Eq. (4), and (ii) if tablet porosity is assumed to constrict and close during the swelling process, i.e., Eq. (7). It is evident from the figures that, regardless of the limiting scenario considered, tablets having a smaller relative density absorb more water at a faster rate. Fig. 15 shows the water absorbed by the pore space under these two limiting scenarios, i.e., Eqs. (3) and (9) are used. If tablet porosity is assumed fixed during swelling, the water absorbed by the pore space initially increases at a nearly constant rate, and it then reaches a maximum (see Fig. 15(a)). If tablet porosity is assumed to constrict and close during swelling, the water absorbed by the pore space reaches a maximum and, eventually, the water is squeezed out before pores close (see Fig. 15(b)). It is evident from the figures that, regardless of the limiting scenario considered, tablets having a smaller relative density absorb more water due to the higher availability of void space. Fig. 16 shows the water absorbed by the excipients. Specifically, if tablet porosity is assumed fixed during swelling, Eq. (2) is used, and the water inside the excipients (i.e., 136.2 mg of Avicel PH 200) is recovered to be independent of tablet relative density or the degree of deformation of the particles in the blend (see Fig. 16(a)). In contrast, if tablet porosity is assumed to constrict and close during swelling, Eq. (8) is used, and the water inside the excipients is recovered to be dependent on tablet relative density (see Fig. 16(b)). It bears emphasis that the results in Fig. 16(a) are not enforced by Eq. (2), but they are rather an outcome of the methodology to interpret the fast time-resolved micro-CT images.

Lastly, Fig. 17 shows the time evolution of crack volume determined using the methodology described in the previous section and Eq. (10). These results indicate that larger cracks are formed in tablets with smaller relative densities. As noted above, cracks form later and take longer to be arrested in tablets with higher relative densities. This observation suggests that tablet disintegration starts earlier at smaller relative densities. Moreover, significant crack formation happens between 90–200 s for tablets with all relative densities. During this period, the rate of water uptake has an increasing trend, as shown in Fig. 5. The figure also suggests that the formation and arresting of crack propagation is a discrete sequence of events during the water absorption process. At smaller tablet densities, the evolution of crack volume resembles a piece-wise constant function, indicating that large cracks rapidly

form and are either arrested or emerge from the domain of the tablet. In contrast, at higher tablet densities, the evolution of crack volume is smoother and comprises smaller cracks. This observation suggests that tablet disintegration is faster and more pronounced at smaller relative densities (see https://doi.org/10.1016/j.ijpharm.2023.123565supplemental material (water absorption videos)). In closing, the connection with tablet disintegration processes is evident, and the utilization of fast time-resolved micro-CT imaging to elucidate these processes is a worthwhile direction for future research.

3.1. Physical interpretation

This section will provide a physical interpretation of the first limiting scenario proposed in Section 2.3 where tablet porosity is assumed fixed during the swelling process. Precisely, we will aim at identifying the water pathways as they fill the pore structure and it is absorbed by the swelling excipients. For the second limiting scenario, porosity is assumed to be a linear function of time, as there is a lack of experimental evidence for how the tablet porosity evolves with time during swelling. Hence, a physical interpretation of the second scenario is not attempted.

Water penetration inside a porous sample due to capillary pressure is typically modeled by the Lucas–Washburn theory (Hamraoui and Nylander, 2002). The rate of water uptake depends on the mean effective capillary radius of the pore structure r_e, the contact angle between the liquid and solid θ, the surface tension of the liquid γ, and the viscosity of the liquid η (Washburn, 1921). Many excipients, such as microcrystalline cellulose, are porous and have an intra-particle pore structure characterized by a mean effective capillary radius r_e^{intra}. Similarly, compacted tablets have an inter-particle pore structure characterized by a mean effective capillary radius r_e^{inter}. Hence, we assume that water is absorbed due to capillary pressure either by the inter- or the intra-particle pore structure of the interconnected network of excipient particles. In addition, we assume that the absorbed water is immediately absorbed by the swelling excipient particles from the inter-particle pore network if the former is true or immediately expelled from the swelling particles into the inter-particle pore structure if the latter is true. Hence, for a given position of the dry–wet interface inside the tablet, we assume that the volume of water absorbed under these two scenarios will be the same, albeit taking place at different time scales since $r_e^{\text{inter}} \gg r_e^{\text{intra}}$ for deformable microcrystalline cellulose particles (similarly, we assume $\epsilon^{\text{inter}} = \epsilon_0 \gg \epsilon_e^{\text{intra}}$). We will then discern between these two scenarios by comparing the mean effective capillary radius r_e estimated from the experimental results presented in Section 3 with predictions of a process-based pore network model construction, as well as experimental measurements.

The height of the liquid front L in a porous medium exposed to liquid from the bottom, i.e., the dry–wet interface, is expressed by the well-known Washburn equation (Washburn, 1921). The rate of liquid penetration $\dot{L}$ is then given by

$$\dot{L} = \frac{\mathrm{d}L}{\mathrm{d}t} = \sqrt{\frac{r_e \gamma \cos\theta}{2\eta}} \frac{1}{2\sqrt{t}} \tag{11}$$

where $r_e = r_h^2/r$ depends on the porosity of the solid, with r_h and r being the mean hydraulic and pore radii. Here, we assume that $r_h = r$ (Golman et al., 2005) (i.e., $r = r_e = r_h$). Braido et al. (2012) studied water penetration into a pharmaceutical tablet using video image processing. They used both the Washburn model and the molecular absorption model (see, e.g., Vesely (2001)) to capture the experimental trend of water penetration depth into the tablet, and they concluded that, for the complex formulation, none of the models is sufficient to capture all different physical mechanisms governing liquid penetration into the tablet. An approach based on Darcy's law has also been used to model liquid penetration into a porous medium (Markl et al., 2017; Masoodi et al., 2007; Markl and Zeitler, 2017) and, as it is also the case of the Washburn equation. It captures the initial phase of the experimental trend, but it does not capture the later phase when water penetration is very slow and reaches a plateau (see Fig. 15(a)).

Here, we couple liquid penetration due to capillary pressure described by the Lucas–Washburn theory with the first-order swelling kinetics of the excipients to provide a physical interpretation of the experimental observations derived from the first limiting scenario proposed in Section 2.3. Therefore, from $\epsilon^{\text{inter}} = \epsilon_0 \gg \epsilon_e^{\text{intra}}$, the volume of water absorbed by the excipients is proportional to the height L, the horizontal cross-sectional area A of the dry tablet and the solid fraction of the solid $(1 - \epsilon_0)$ (Hattori and Otsuka, 2011; Otsuka et al., 2014), that is

$$\begin{aligned} V_{\text{water}}^{\text{exc}}(t) &= \underbrace{\sqrt{\frac{r_e\gamma\cos\theta}{2\eta}}\int_0^{\tau}\frac{A(1-\epsilon_0)}{2\sqrt{\hat{t}}}}_{\text{wet solid: capillary intake}}\left[x_{\text{exc}}\underbrace{\text{WAC}\frac{\rho_{\text{true}}}{\rho_{\text{H}_2\text{O}}}\left(1-e^{-k(t-\hat{t})}\right)}_{\text{swelling kinetics}}\right]\mathrm{d}\hat{t} \\ &= (1-\epsilon_0)\sqrt{\frac{A^2 r_e\gamma\cos\theta\,\tau}{2\eta}}x_{\text{exc}}WAC\frac{\rho_{\text{true}}}{\rho_{\text{H}_2\text{O}}}\left(1-\frac{F\left(\sqrt{k\tau}\right)}{\sqrt{k\tau}}e^{-k(t-\tau)}\right) \\ \text{with}\quad \tau &= \min\left[t, 2H^2\eta/r_e\gamma\cos\theta\right] \end{aligned} \tag{12}$$

where $F(\cdot)$ is the Dawson integral, $x_{\text{exc}} = 0.89$ is the concentration (w/w) of the excipients that undergo swelling, and $2H^2\eta/r_e\gamma\cos\theta$ is the time of arrival of the wet front to the top surface of the tablet with dry height H. The only ingredient in the current formulation that swells is Avicel PH 200. In the above equation, WAC% is the water absorption capacity of the excipients, $\rho_{\text{H}_2\text{O}} = 1\ \text{mg/mm}^3$ is the density of water, $\rho_{\text{true}} = 1.53\ \text{mg/mm}^3$ is the true density of the powder blend, k is the swelling rate constant for the first-order swelling kinetics (Schott, 1992a,b). WAC (w/w) is a material property that expresses the maximum water absorbed by a material as a percent of dry mass (Witono et al., 2014). Similarly, the water inside the pore space is given by

$$V_{\text{water}}^{void}(t) = \underbrace{\epsilon_0\sqrt{\frac{A^2 r_e\gamma\cos\theta\,\tau}{2\eta}}\left[1+\underbrace{x_{\text{exc}}WAC\frac{\rho_{\text{true}}}{\rho_{\text{H}_2\text{O}}}\left(1-\frac{F(\sqrt{k\tau})}{\sqrt{k\tau}}e^{-k(t-\tau)}\right)}_{\text{swollen fraction}}\right]}_{\text{total volume of the tablet after swelling}}$$

(13)

Hence, the total volume of water inside the tablet is

$$V_{\text{water}}(t) = V_{\text{water}}^{\text{exc}}(t) + V_{\text{water}}^{\text{void}}(t) = \sqrt{\frac{A^2 r_e \gamma \cos\theta\tau}{2\eta}}\left[\epsilon_0 + x_{\text{exc}}\text{WAC}\frac{\rho_{\text{true}}}{\rho_{\text{H}_2\text{O}}}\left(1 - \frac{F\left(\sqrt{k\tau}\right)}{\sqrt{k\tau}}\text{e}^{-k(t-\tau)}\right)\right] \tag{14}$$

A parameter identification method has been developed based on a nonlinear multivariate minimization problem. The method minimizes the sum of squared error SSE between experimental data $\mathscr{E}^i$ and model predictions $\mathscr{M}^i$ by choosing optimal model parameters $\overline{\mathscr{P}}$, that is

$$\overline{\mathscr{P}} = \arg\min_{\mathscr{P} \in \mathbb{R}_+} \boldsymbol{\Phi}(\mathscr{P}) = \arg\min_{\mathscr{P} \in \mathbb{R}_+} \sum_{i=1}^{n} \left(\mathscr{M}^i(\mathscr{P}) - \mathscr{E}^i\right)^2 \tag{15}$$

where n is the total number of experimental data points. The set of model parameters is given by

$$\mathscr{P} \equiv \{\text{WAC}, k, r_e(\epsilon)\} \tag{16}$$

The nonlinear multivariate minimization problem was solved in MATLAB (MATLAB version 9.8.0.1380330 (R2020a), 2020) using the constrained optimization function `fmincon` with the default interior-point algorithm. Specifically, by using the properties of the powder blend, the tablet, and the liquid, Eqs. (12) and (13) are used with the experimental data in Figs. 16(a) and 15(a), respectively, to estimate model parameters WAC, k, and r_e (see Tables 2 and 3). The agreement between the model and the experimental data is remarkable, as shown in 18, except for the period when the rate of water uptake was observed to exhibit a non-monotonic trend and cracks form (cf. Figs. 4, 5, and 17, and the discussion in Section 3).

The estimation of confidence intervals of model predictions is described next in turn. First, we incorporate the error of the experimental data by forward uncertainty propagation (Owen, 2013; Guo, 2020). We assume the forward uncertainty follows a normal distribution with 95% confidence interval lying within the experimental error bound. The influence of the error of input data through the models to output model parameters is then evaluated by propagating the error with a Monte Carlo simulation approach (Anderson, 1976; Hong et al., 2006). At the end of this step, we obtain an ensemble of estimated model parameters which has uncertainty coming from model predictions. The covariance matrix for each set of model parameters is approximated as

$$\mathrm{cov}_{\bar{\mathscr{P}}} \approx \frac{\boldsymbol{\Phi}(\bar{\mathscr{P}})}{\mathrm{dof}} [\nabla^2 \boldsymbol{\Phi}(\bar{\mathscr{P}})]^{-1} \tag{17}$$

where the objective function $\boldsymbol{\Phi}$, i.e., Eq. (15), and its Hessian $\nabla^2\boldsymbol{\Phi}$ are evaluated at the optimal model parameters $\bar{\mathscr{P}}$ (see, e.g., Casas-Orozco et al. (2021), Barz et al. (2015), Fessler (1996) and Ferdoush and Gonzalez (2023)). In the above equation, the degrees of freedom dof are the difference between the number of data points and the number of model parameters. It is worth noting that the covariance matrix is non-diagonal, i.e., model parameters are correlated with respect to each Gaussian random variable $\mathcal{N}(\bar{\mathscr{P}}, \mathrm{cov}_{\bar{\mathscr{P}}})$. The parameters are sampled other. Hence, we assume that the model parameters are multivariate using a Monte Carlo approach to derive 95% confidence intervals of model functions $V^{\mathrm{void}}_{\mathrm{water}}(t)$ and $V^{\mathrm{exc}}_{\mathrm{water}}(t)$, as shown in Fig. 18.

If tablet porosity is assumed fixed during the swelling process, estimations shown in Fig. 16(a) indicate that the water absorbed by the excipient is independent of tablet relative density or the level of densification of the material. This swelling behavior is characterized by WAC (w/w). Tomer et al. (2001) reported water retention of Avicel PH 102 particles equal to 64.4% from samples centrifuged for 30 min at 5500 rpm. Nikolakakis et al. (2006) studied that the water retention of Avicel PH 101 tablets changes with centrifugation time if centrifuged at 2500 rpm for less than 5 min and that otherwise, changes are negligible. Evidently, the water retention of Avicel PH 102 particles or Avicel PH 101 tablets after centrifugation, and the water absorption capacity of Avicel PH 200 tablets are not comparable. However, microcrystalline cellulose water retention values reported in the literature are close to the WAC values estimated for the tablets studied in this work, i.e., to 79% (see Table 2).

The estimated value of k is 0.10 1/s, which is close to the values found in the literature. Bahadoran Baghbadorani et al. (2020) reported 0.016 1/s as the value of k for hydrogel with 5% reinforced cellulose nano fiber. Ogawa et al. (1993) reported a swelling rate constant in the order of 0.01 1/s for sodium polyacrylate, which is a hydrophilic polymer.

The estimated capillary radii r_e (see Table 3) are of the same order of magnitude of the value 9.8 nm estimated by Markl et al. (2017) from the Washburn equation for radially confined tablets made of 100% Avicel PH 102 and porosity 0.10. It is worth noting that Avicel PH 200 and Avicel PH 102 have different particle size distributions—with a mean particle size of 200 μm ((Pharma), 2020) for the former and 100 μm (Markl et al., 2017) for the latter. In addition, Martins and Gonzalez (2022) used a process-based pore network model to show that the inter-particle hydraulic radius is approximately 1% of the particle size for a die-compacted monodisperse spherical packing (Fig. 19). This process-based method applies to granular packings under large deformations and it uses the particle mechanics approach for modeling the consolidation of powders under large deformations (Gonzalez and Cuitino, 2012; Gonzalez and Cuitiño, 2016; Yohannes et al., 2016, 2017; Gonzalez, 2019). Therefore, we conclude that water penetration is dominated by intra-particle porosity,

rather than inter-particle porosity since the effective capillary radius r_e is 0.0037% of the mean particle size.

It bears emphasis that the agreement between estimated model parameters and values reported in the literature is solely derived from the time-resolved micro-CT images adopting the assumption that tablet porosity is fixed during the swelling process, which is suggestive of the validity of the assumption as well as the feasibility of the imaging technique to investigate water uptake, swelling and disintegration of immediate-release pharmaceutical tablets.

4. Conclusion

We have used dynamic micro-CT with a high temporal resolution to visualize water penetration through the porous network of immediate-release pharmaceutical solid tablets and characterize dynamic swelling and disintegration mechanisms. We have processed the micro-CT images using two theoretical limiting scenarios that reflect different paths of pore structure evolution: a scenario where tablet porosity remains constant during the swelling process and a scenario where the tablet porosity progressively diminishes and eventually closes during the swelling process. We have calculated the time evolution of the volume of water absorbed by the tablet and, specifically, absorbed by the excipients and by the pore structure, as well as the formation and evolution of cracks. In turn, the three-dimensional disintegration pattern of the tablets was reconstructed. Regardless of the limiting scenario, tablets with smaller relative densities absorb more water due to the higher availability of void space. Moreover, larger cracks are formed in tablets with smaller relative densities. This observation suggests that tablet disintegration is faster and more pronounced at smaller relative densities. Restricting attention to the limiting scenario where tablet porosity is assumed fixed during the swelling process, we have proposed a model that couples liquid penetration due to capillary pressure described by the Lucas–Washburn theory with the first-order swelling kinetics of the excipients to provide a physical interpretation of the experimental observations. The model assumes that swelling kinetics starts as soon as the water is absorbed by the interconnected network of excipients particles, either through inter-particle or intra-particle porosity. Next, we have developed a parameter identification method based on a nonlinear multivariate minimization problem of the SSE between water absorption experimental data and model predictions. The estimated model parameters are in agreement with values reported in the literature, and they indicate that water penetration is dominated by intra-particle porosity rather than inter-particle porosity. Lastly, it is worth noting that the agreement between estimated model parameters and values reported in the literature was solely derived from the time-resolved micro-CT images adopting the assumption that tablet porosity is fixed during the swelling process, which is suggestive of the validity of the assumption as well as the feasibility of the imaging technique to investigate water uptake, swelling and disintegration of immediate-release pharmaceutical tablets.

Supplementary Material

Refer to Web version on PubMed Central for supplementary material.

Acknowledgments

The motivation for this work arose from a special topics course for undergraduate students, ME479, on *dynamic micro-CT imaging of swelling and disintegration processes in pharmaceutical tablets* given as an independent research project at the School of Mechanical Engineering at Purdue University. Sarah Bu Kzam was a participant from the spring of 2021 to the spring of 2022. This research is supported by the National Science Foundation grant number CMMI-1538861, entitled “Understanding the effect of powder properties and processing conditions on the performance of pharmaceutical tablets”, and by the U.S. Food and Drug Administration through grant number 1U01FD006738-01, 5U01FD006738-02, and 5U01FD006738-03 entitled “Risk-based process synthesis and Industry 4.0 framework for pharmaceutical manufacturing processes”. The authors gratefully acknowledge Gamlen Instruments (London, UK) for the availability of the Gamlen D Series bench-top compaction simulator and Object Research Systems Inc. for the academic license of Dragonfly.

Data availability

Data will be made available on request.

References

Abdul S, Poddar S, 2004. A flexible technology for modified release of drugs: multi layered tablets. J. Control. Release 97 (3), 393–405. [PubMed: 15212872]

Anderson G, 1976. Error propagation by the Monte Carlo method in geochemical calculations. Geochim. Cosmochim. Acta 40 (12), 1533–1538.

Augsburger LL, Zellhofer MJ, Swarbick J, Boylan J, 2007. Tablet formulation. Encyclopedia Pharm. Technol. 3.

Bahadoran Baghbadorani N, Behzad T, Karimi Darvanjooghi MH, Etesami N, 2020. Modelling of water absorption kinetics and biocompatibility study of synthesized cellulose nanofiber-assisted starch-graft-poly (acrylic acid) hydrogel nanocomposites. Cellulose 27, 9927–9945.

Barz T, Körkel S, Wozny G, et al. , 2015. Nonlinear ill-posed problem analysis in model-based parameter estimation and experimental design. Comput. Chem. Eng. 77, 24–42.

Boever WD, Dewanckele J, Hümbert M, Grießer A, Rief S, Ferdoush S, Martins P, Gonzalez M, 2021. Dynamic micro-CT: Nondestructive imaging in the fourth dimension. Microsc. Anal..

Braido D, Gulak Y, Cuitino A, 2012. Solvent penetration rate in tablet measurement using video image processing. AAPS PharmSciTech 13, 507–512. [PubMed: 22426793]

Butenegro JA, Bahrami M, Swolfs Y, Ivens J, Martínez MÁ, Abenojar J, 2022. Novel thermoplastic composites strengthened with carbon fiber-reinforced epoxy composite waste rods: Development and characterization. Polymers 14 (19), 3951. [PubMed: 36235899]

Casas-Orozco D, Laky D, Wang V, Abdi M, Feng X, Wood E, Laird C, Reklaitis GV, Nagy ZK, 2021. PharmaPy: An object-oriented tool for the development of hybrid pharmaceutical flowsheets. Comput. Chem. Eng. 153, 107408.

Costa P, Lobo JMS, 2001. Modeling and comparison of dissolution profiles. Eur. J. Pharm. Sci. 13 (2), 123–133. [PubMed: 11297896]

Desai PM, Liew CV, Heng PWS, 2016. Review of disintegrants and the disintegration phenomena. J. Pharm. Sci. 105 (9), 2545–2555. [PubMed: 27506604]

Dewanckele J, Boone M, Coppens F, Van Loo D, Merkle A, 2020. Innovations in laboratory-based dynamic micro-CT to accelerate in situ research. J. Microsc. 277 (3), 197–209. [PubMed: 32073655]

Dewanckele J, Coppens F, De Boever W, Boone M, Hunter L, 2021. In situ dynamic X-ray micro-CT for additive manufactured parts. Microsc. Microanal. 27 (S1), 2944–2945.

2022. Dragonfly 2022.1 [Computer Software] [Computer Software Manual]. Montreal, Canada.

Eiliazadeh B, Briscoe BJ, Sheng Y, Pitt K, 2003. Investigating density distributions for tablets of different geometry during the compaction of pharmaceuticals. Particul. Sci. Technol. 21 (4), 303–316.

Faroongsarng D, Peck GE, 1994. The swelling & water uptake of tablets III: moisture sorption behavior of tablet disintegrants. Drug Dev. Ind. Pharm. 20 (5), 779–798.

Ferdoush S, Gonzalez M, 2023. Semi-mechanistic reduced order model of pharmaceutical tablet dissolution for enabling industry 4.0 manufacturing systems. Int. J. Pharm. 631, 122502. [PubMed: 36529354]

Fessler J, 1996. Mean and variance of implicitly defined biased estimators (such as penalized maximum likelihood): applications to tomography. IEEE Trans. Image Process. 5 (3), 493–506. 10.1109/83.491322. [PubMed: 18285134]

Golman B, Takigawa T, Shinohara K, Ohzeki K, 2005. Kinetics of liquid penetration into bottom edge of cast tape. Colloids Surf. A 254 (1–3), 9–16.

Gonzalez M, 2019. Generalized loading-unloading contact laws for elasto-plastic spheres with bonding strength. J. Mech. Phys. Solids 122, 633–656.

Gonzalez M, Cuitino AM, 2012. A nonlocal contact formulation for confined granular systems. J. Mech. Phys. Solids 60 (2), 333–350.

Gonzalez M, Cuitiño AM, 2016. Microstructure evolution of compressible granular systems under large deformations. J. Mech. Phys. Solids 93, 44–56.

Guo S, 2020. Using Monte Carlo to quantify the model prediction error. https://towardsdatascience.com/how-to-quantify-the-prediction-error-made-by-my-model-db4705910173. (Accessed on 09/19/2023).

Hamraoui A, Nylander T, 2002. Analytical approach for the Lucas–Washburn equation. J. Colloid Interface Sci. 250 (2), 415–421. [PubMed: 16290679]

Hattori Y, Otsuka M, 2011. NIR spectroscopic study of the dissolution process in pharmaceutical tablets. Vib. Spectrosc. 57 (2), 275–281.

Hong Y, Hsu K. l., Moradkhani H, Sorooshian S, 2006. Uncertainty quantification of satellite precipitation estimation and Monte Carlo assessment of the error propagation into hydrologic response. Water Resour. Res. 42 (8).

Hunter L, Dewanckele J, 2021. Evolution of micro-CT: Moving from 3D to 4D. Microsc. Today 29 (3), 28–34.

Javanshour F, Prapavesis A, Lahtonen K, Pournoori N, Pärnänen T, Kanerva M, Van Vuure AW, Sarlin E, 2023. Effect of graphene oxide fibre surface modification on low-velocity impact and fatigue performance of flax fibre reinforced composites. Composites C 11, 100360.

Joseph M, Van Cauteren H, Postelmans A, Nugraha B, Verreydt C, Verboven P, Nicolai B, Saeys W, 2023. Porosity quantification in pear fruit with X-ray CT and spatially resolved spectroscopy. Postharvest Biol. Technol. 204, 112455.

Kottke MJ, Rudnic EM, 2002. Tablet dosage forms. In: Modern Pharmaceutics. CRC Press, pp. 458–532.

Kristó K, Bajdik J, Kleinebudde P, Pintye-Hódi K, 2010. Effect of lubricant on spreading of coating liquid on surface of tablets containing pancreatin. Pharm. Dev. Technol. 15 (4), 354–359. [PubMed: 19772392]

Markl D, Yassin S, Wilson DI, Goodwin DJ, Anderson A, Zeitler JA, 2017. Mathematical modelling of liquid transport in swelling pharmaceutical immediate release tablets. Int. J. Pharm. 526 (1–2), 1–10. [PubMed: 28400289]

Markl D, Zeitler JA, 2017. A review of disintegration mechanisms and measurement techniques. Pharm. Res. 34 (5), 890–917. [PubMed: 28251425]

Martins PH, Gonzalez M, 2022. A process-based pore network model construction for granular packings under large plastic deformations. Transp. Porous Media 1–28.

Masoodi R, Pillai KM, Varanasi PP, 2007. Darcy's law-based models for liquid absorption in polymer wicks. AIChE J. 53 (11), 2769–2782.

2020. MATLAB Version 9.8.0.1380330 (R2020a) [Computer Software Manual]. Natick, Massachusetts.

Mesquita F, Melnikov A, Rajpurohit A, Singery V, Sanial P, Lomov SV, Swolfs Y, 2022. Tensile failure strain and microstructure of unidirectional carbon fibre non-crimp fabric composites. Composites B 243, 110123.

Moreton RC, 2008. Disintegrants in tableting. In: Pharmaceutical Dosage Forms-Tablets. CRC Press, pp. 233–266.

Nikolakakis I, Tsarvouli K, Malamataris S, 2006. Water retention and drainage in different brands of microcrystalline cellulose: Effect of measuring conditions. Eur. J. Pharm. Biopharm. 63 (3), 278–287. [PubMed: 16527466]

Ogawa I, Yamano H, Miyagawa K, 1993. Rate of swelling of sodium polyacrylate. J. Appl. Polym. Sci. 47 (2), 217–222.

Otsuka M, Kanai Y, Hattori Y, 2014. Real-time monitoring of changes of adsorbed and crystalline water contents in tablet formulation powder containing theophylline anhydrate at various temperatures during agitated granulation by near-infrared spectroscopy. J. Pharm. Sci. 103 (9), 2924–2936. [PubMed: 24832393]

Owen AB, 2013. Monte Carlo Theory, Methods and Examples. Stanford.

Peppas NA, Narasimhan B, 2014. Mathematical models in drug delivery: How modeling has shaped the way we design new drug delivery systems. J. Control. Release 190, 75–81. [PubMed: 24998939]

(Pharma) D, 2020. Avicel® selection guide.

Pinto JC, de Faria-Vasconcelos K, Leite AF, Pedano MS, Guerreiro-Tanomaru J, Jacobs R, Tanomaru-Filho M, 2023. Effect of foraminal enlargement on microcrack formation and apical transportation: a nano-CT assessment. Sci. Rep. 13 (1), 4881. [PubMed: 36966188]

Quodbach J, Kleinebudde P, 2016. A critical review on tablet disintegration. Pharm. Dev. Technol. 21 (6), 763–774. [PubMed: 25975586]

Rosiaux Y, Jannin V, Hughes S, Marchaud D, 2014. Solid lipid excipients—Matrix agents for sustained drug delivery. J. Control. Release 188, 18–30. [PubMed: 24929038]

Rowe RC, Sheskey P, Quinn M, 2009. Handbook of Pharmaceutical Excipients. Libros Digitales-Pharmaceutical Press.

Rudnic E, Rhodes C, Welch S, Bernardo P, 1982. Evaluations of the mechanism of disintegrant action. Drug Dev. Ind. Pharm. 8 (1), 87–109.

Schott H, 1992a. Kinetics of swelling of polymers and their gels. J. Pharm. Sci. 81 (5), 467–470. [PubMed: 1403682]

Schott H, 1992b. Swelling kinetics of polymers. J. Macromol. Sci. B: Phys. 31 (1), 1–9.

Schuchard DR, Berg JC, 1991. Liquid transport in composite cellulose—superabsorbent fiber networks. Wood Fiber Sci. 342–357.

Siepmann J, Peppas NA, 2012. Modeling of drug release from delivery systems based on hydroxypropyl methylcellulose (HPMC). Adv. Drug Deliv. Rev. 64, 163–174.

Soundaranathan M, Vivattanaseth P, Walsh E, Pitt K, Johnston B, Markl D, 2020. Quantification of swelling characteristics of pharmaceutical particles. Int. J. Pharm. 590, 119903. [PubMed: 32980508]

Steele DF, Moreton RC, Staniforth JN, Young PM, Tobyn MJ, Edge S, 2008. Surface energy of microcrystalline cellulose determined by capillary intrusion and inverse gas chromatography. AAPS J. 10, 494–503. [PubMed: 18841480]

Suzuki K, Yoshiki M, Nishikawa N, Harada T, Fujita Y, Terui Y, Yoshida T, Tomita T, 2022. Visualizing fluid transport inside orally disintegrating tablets and changes in tablets using real-time X-ray radiography and X-ray computed tomography. Drug Dev. Ind. Pharm. 48 (7), 301–309. [PubMed: 35913028]

Tomer G, Patel H, Podczeck F, Newton J, 2001. Measuring the water retention capacities (MRC) of different microcrystalline cellulose grades. Eur. J. Pharm. Sci. 12 (3), 321–325. [PubMed: 11113651]

Vacuum P, 2022. Royal microscopy society. Microsc. Today.

van der Wal D, 2021. Time-resolved dynamic X-ray micro-CT: Shifting the focus from material characterization to material behavior.

Vesely D, 2001. Molecular sorption mechanism of solvent diffusion in polymers. Polymer 42 (9), 4417–4422.

Washburn EW, 1921. The dynamics of capillary flow. Phys. Rev. 17 (3), 273.

Wen H, Park K, 2011. Oral Controlled Release Formulation Design and Drug Delivery: Theory to Practice. John Wiley & Sons.

Witono JR, Noordergraaf I, Heeres H, Janssen L, 2014. Water absorption, retention and the swelling characteristics of cassava starch grafted with polyacrylic acid. Carbohydr. Polym. 103, 325–332. [PubMed: 24528736]

Yohannes B, Gonzalez M, Abebe A, Sprockel O, Nikfar F, Kiang S, Cuitiño A, 2016. Evolution of the microstructure during the process of consolidation and bonding in soft granular solids. Int. J. Pharm. 503 (1–2), 68–77. [PubMed: 26902721]

Yohannes B, Gonzalez M, Abebe A, Sprockel O, Nikfar F, Kiang S, Cuitiño A, 2017. Discrete particle modeling and micromechanical characterization of bilayer tablet compaction. Int. J. Pharm. 529 (1–2), 597–607. [PubMed: 28713000]

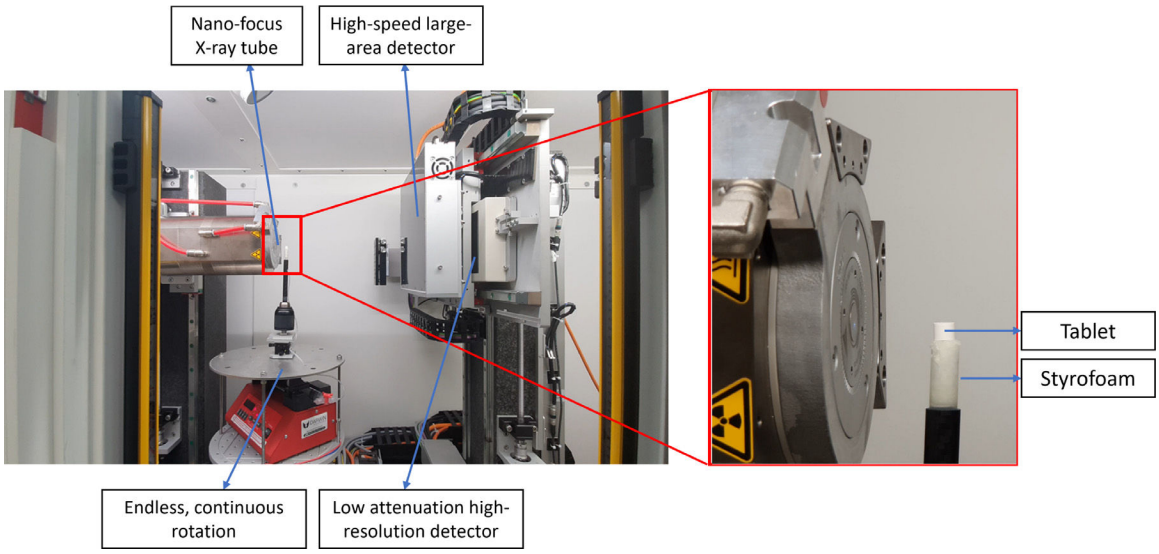

Fig. 1.

Experimental setup of TESCAN UniTOM HR. The tablet absorbs water from the styrofoam. The tablet is rotated uninterruptedly with the help of the rotating table. High temporal resolution and continuous scanning of the entire water absorption process were obtained using the state-of-the-art nano-focus X-ray source and high-quality detectors.

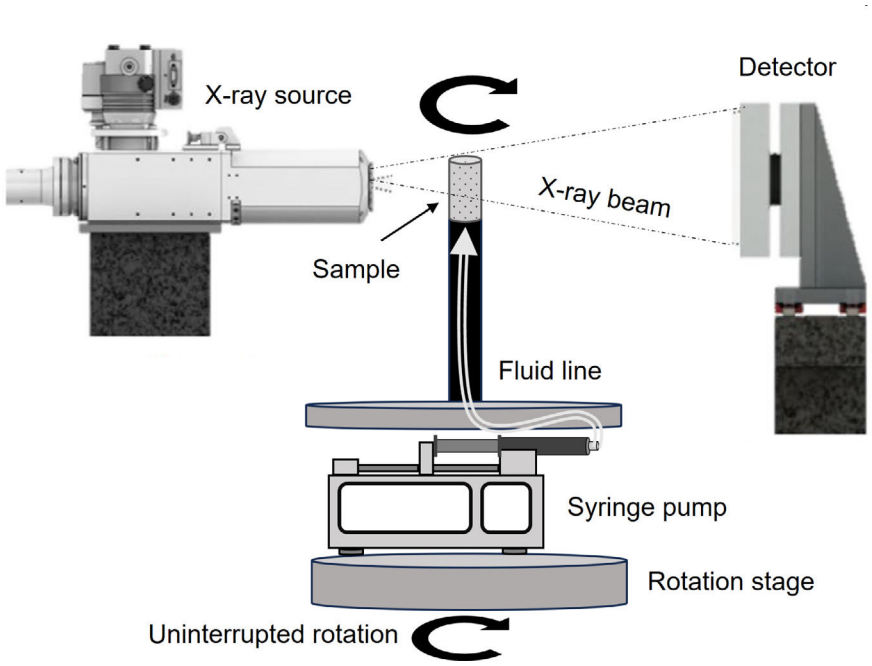

Fig. 2.
Schematic of TESCAN UniTOM HR.

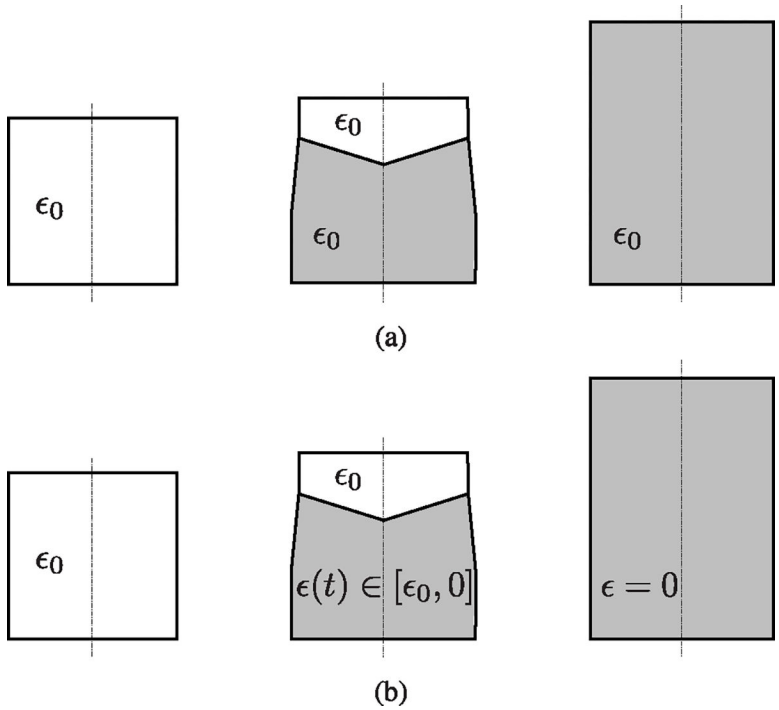

Fig. 3.

Simplified schematic of a dry and wet/swollen tablet. The white area represents dry tablet, and the gray area represents wet and swollen tablet. (a) Porosity is assumed fixed during swelling, the pore space of the dry area is filled with air, and the wet area is filled with water. (b) Porosity is assumed to close during swelling, the pore space of the dry area is filled with air, and the wet area does not have any pore space at steady state conditions.

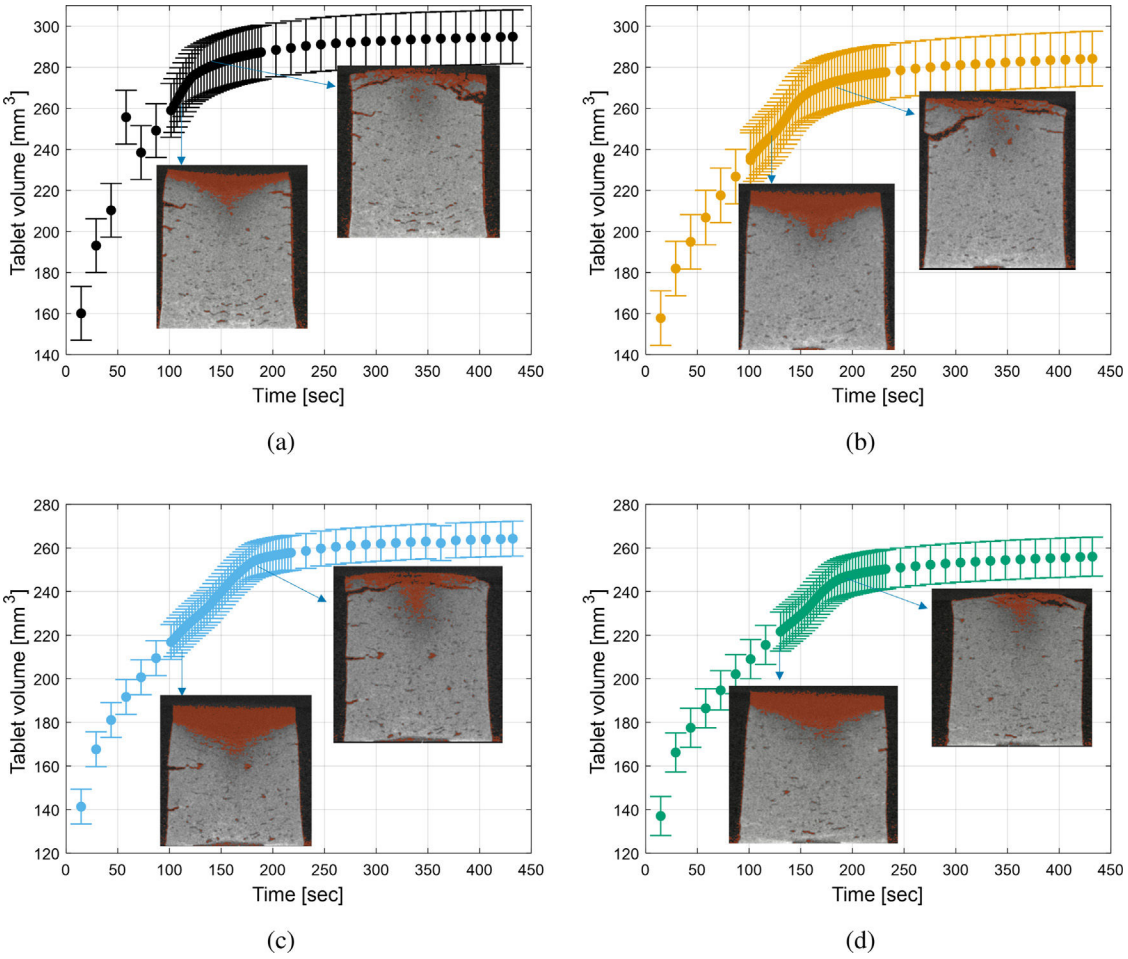

Fig. 4.

Time evolution of total tablet volume. Inserts depict snapshots of tablet cross-section with dry (orange) and wet/swollen (gray) regions taken at the beginning and at the end of the non-monotonic region in water uptake rate. (a) $\rho_{\text{in-die}} = 0.80$, snapshot at 110.2 and 147.9 s. (b) $\rho_{\text{in-die}} = 0.85$, snapshots at 121.8 and 176.9 s. (c) $\rho_{\text{in-die}} = 0.90$, snapshots at 113.1 and 182.7 s. (d) $\rho_{\text{in-die}} = 0.95$, snapshots at 130.5 and 197.2 s.

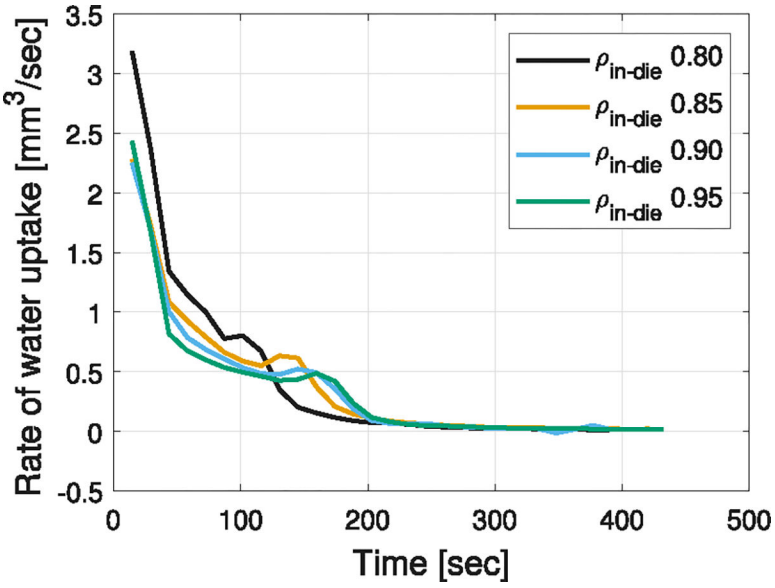

Fig. 5.
Rate of water uptake.

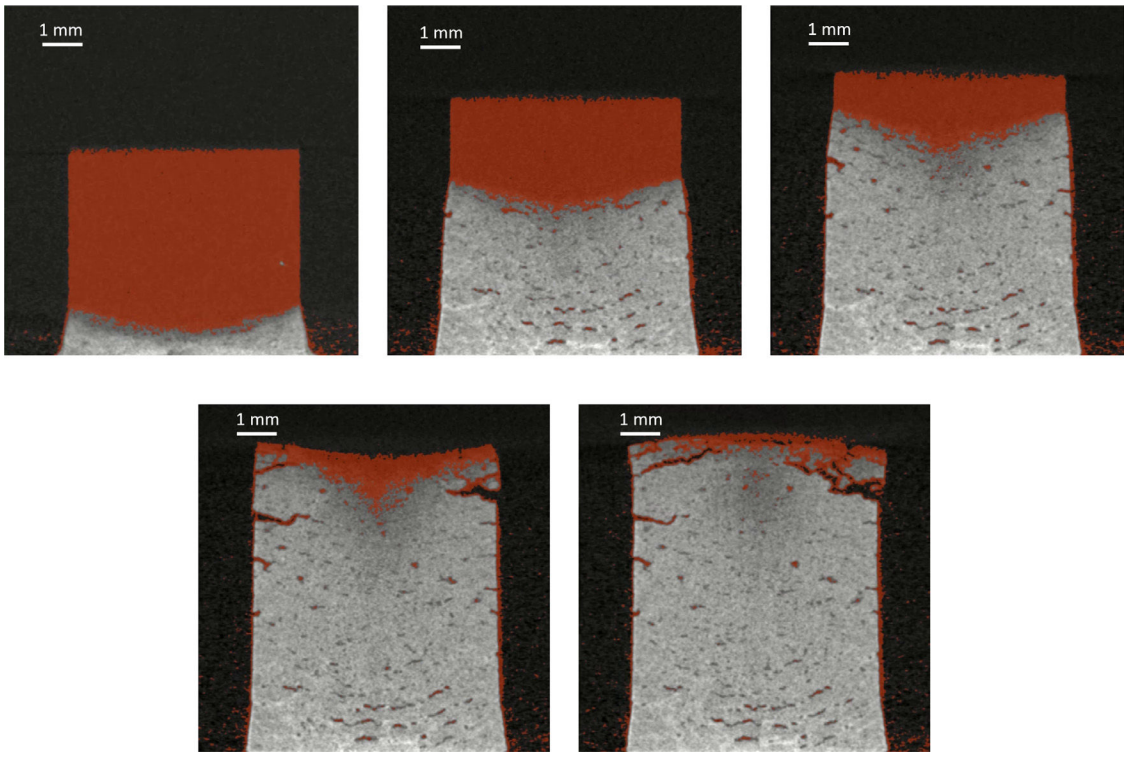

Fig. 6.

Fast water uptake by tablet of relative density 0.80. Orange corresponds to the dry tablet and gray corresponds to wet and swollen tablet. Images show water absorption at timestamps 14.5, 52.2, 89.9, 118.9 and 153.7 s.

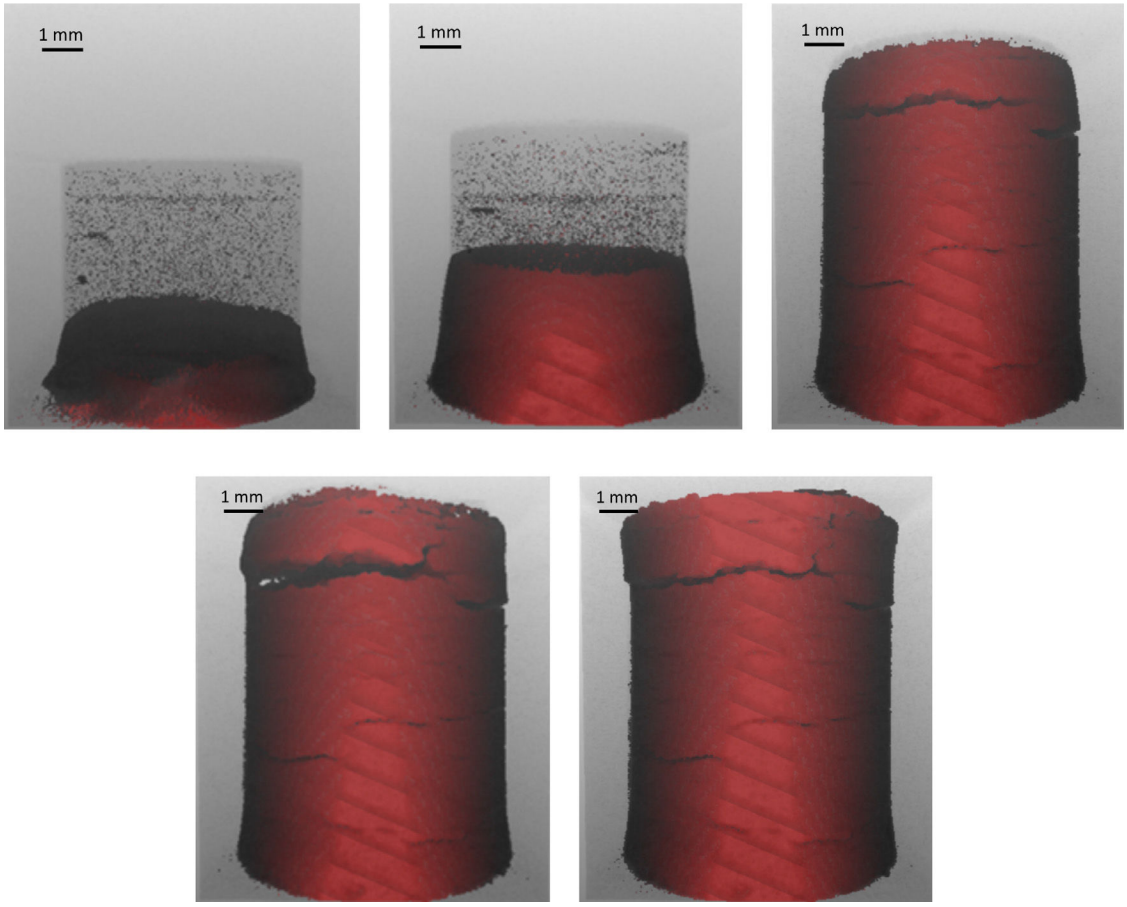

Fig. 7.

Fast water uptake by tablet of relative density 0.80. Dark gray corresponds to the dry tablet and red corresponds to wet and swollen tablet. Images show water absorption at timestamps 14.5, 29, 110.2, 121.8, and 348 s.

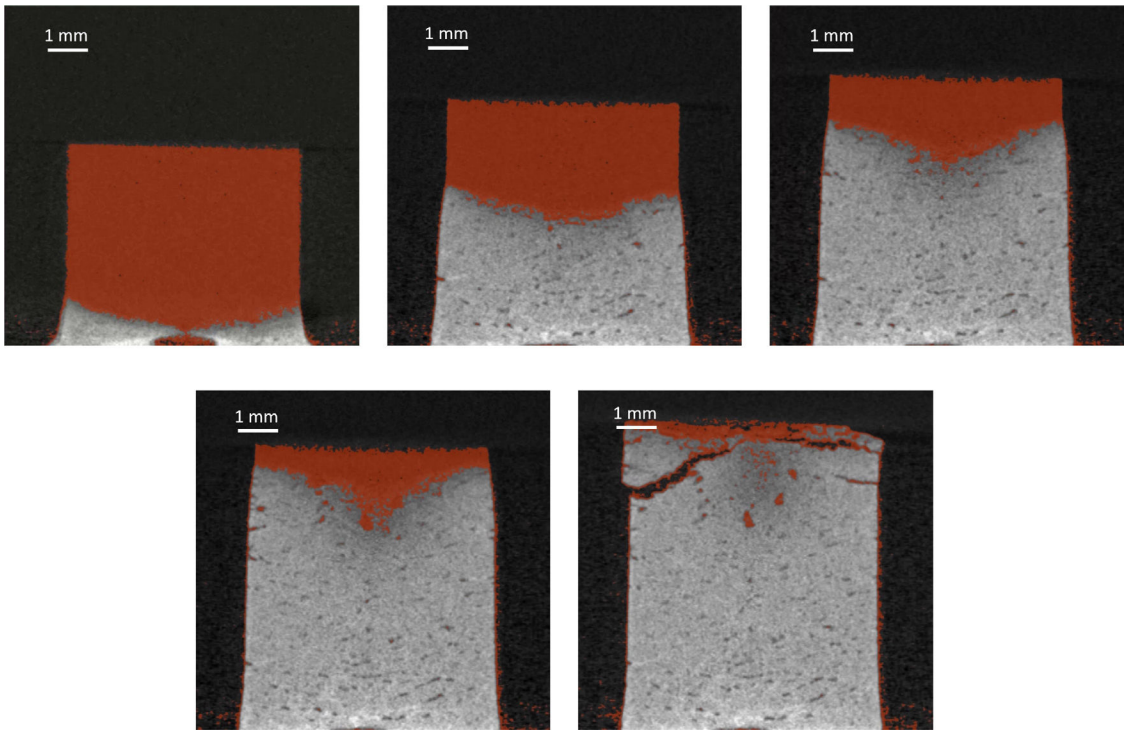

Fig. 8.

Fast water uptake by tablet of relative density 0.85. Orange corresponds to the dry tablet and gray corresponds to wet and swollen tablet. Images show water absorption at timestamps 14.5, 52.2, 92.8, 130.5 and 185.6 s.

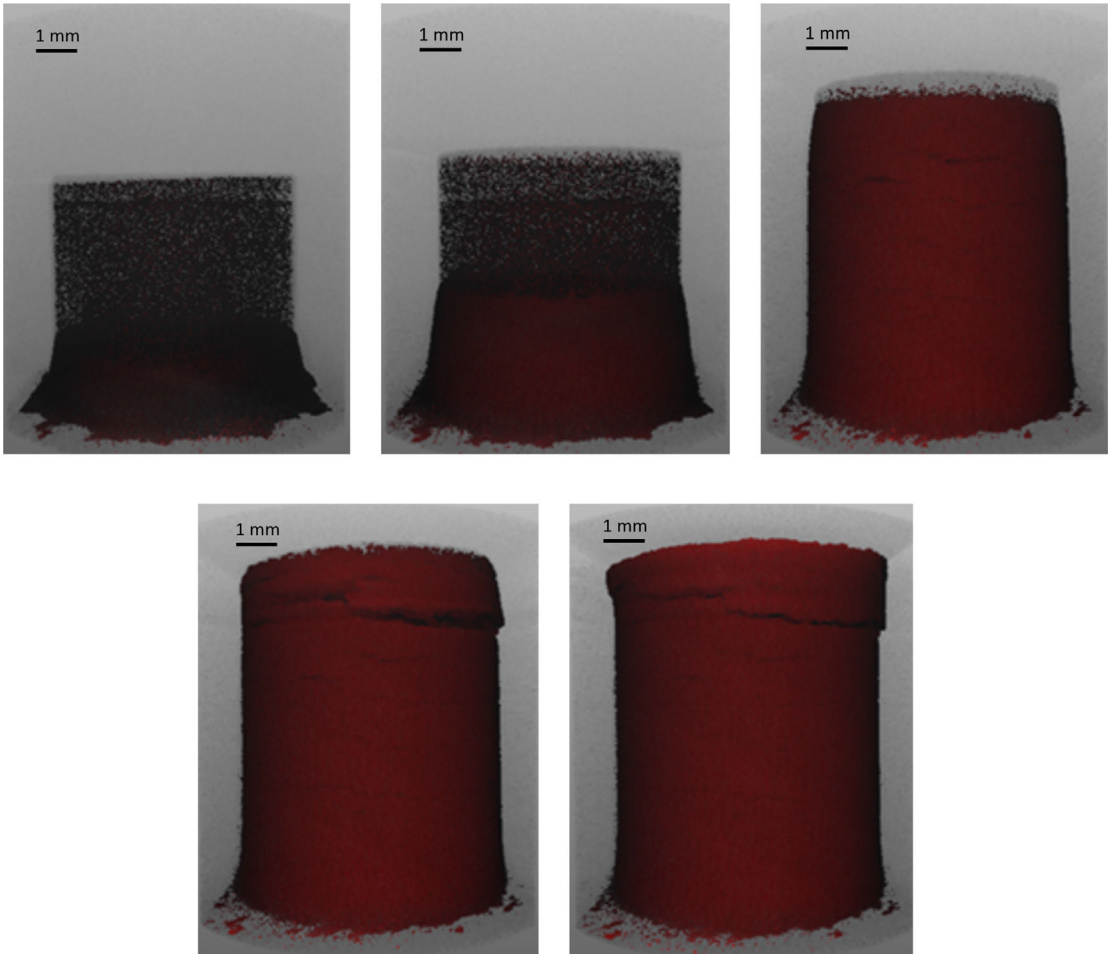

Fig. 9.

Fast water uptake by tablet of relative density 0.85. Dark gray corresponds to the dry tablet and red corresponds to wet and swollen tablet. Images show water absorption at timestamps 14.5, 29, 121.8, 147.9 and 382.8 s.

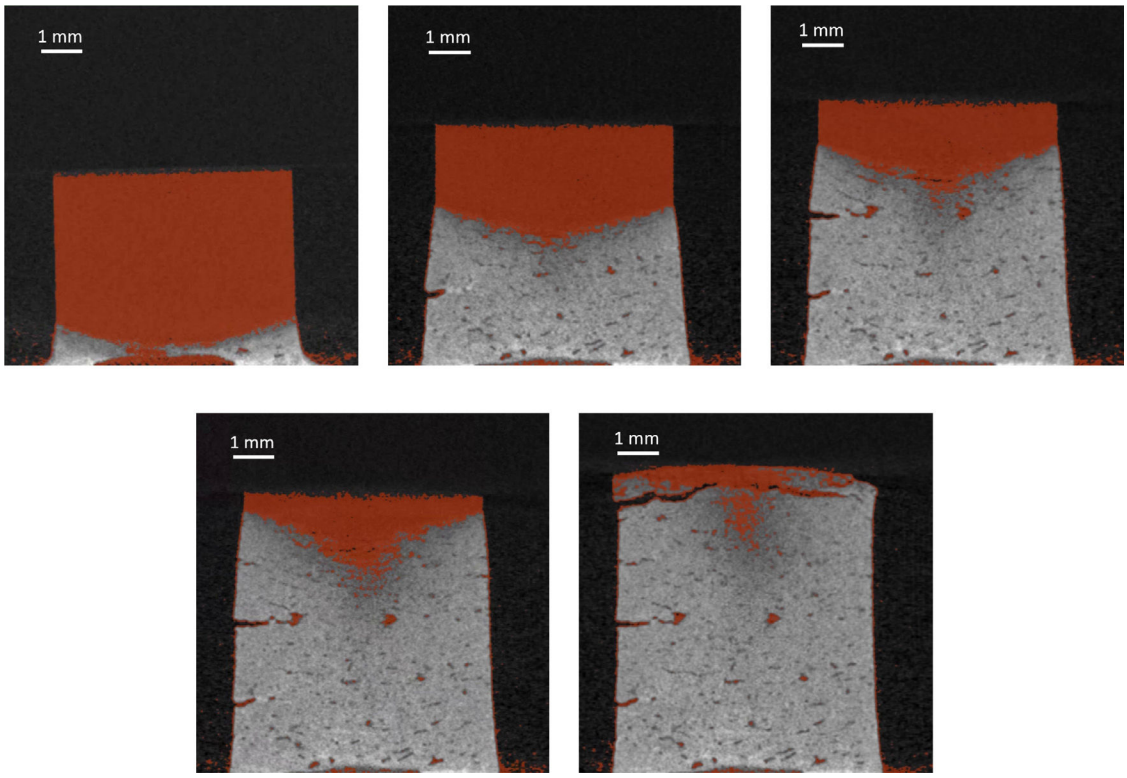

Fig. 10.

Fast water uptake by tablet of relative density 0.90. Orange corresponds to the dry tablet and gray corresponds to wet and swollen tablet. Images show water absorption at timestamps 14.5, 52.2, 95.7, 127.6 and 188.5 s.

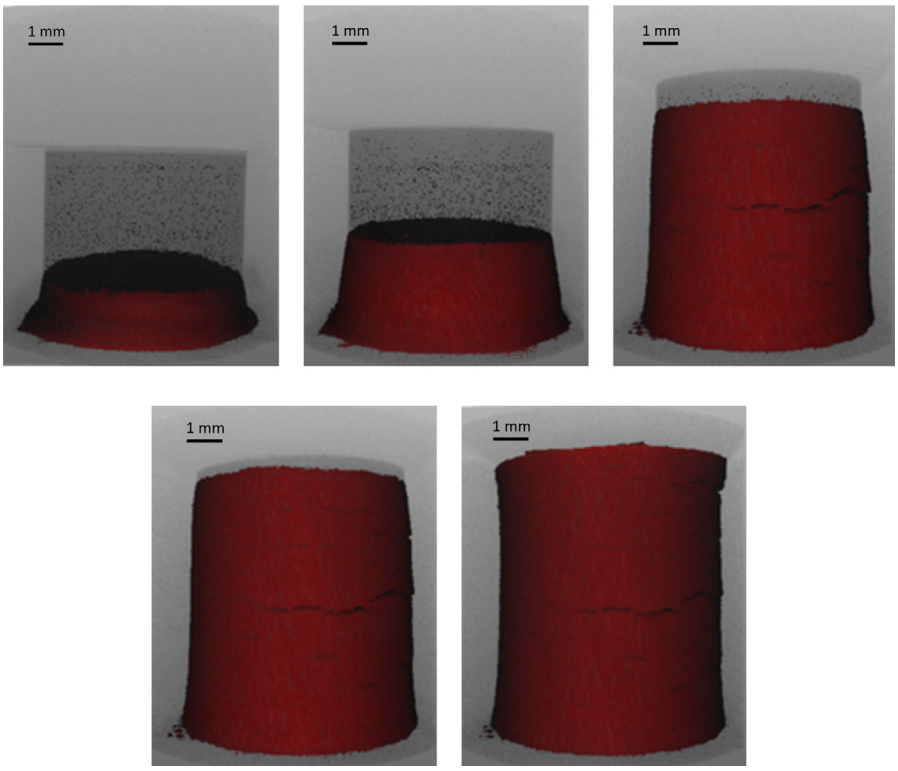

Fig. 11.

Fast water uptake by tablet of relative density 0.90. Dark gray corresponds to the dry tablet and red corresponds to wet and swollen tablet. Images show water absorption at timestamps 14.5, 29, 113.1, 142.1, and 295.8 s.

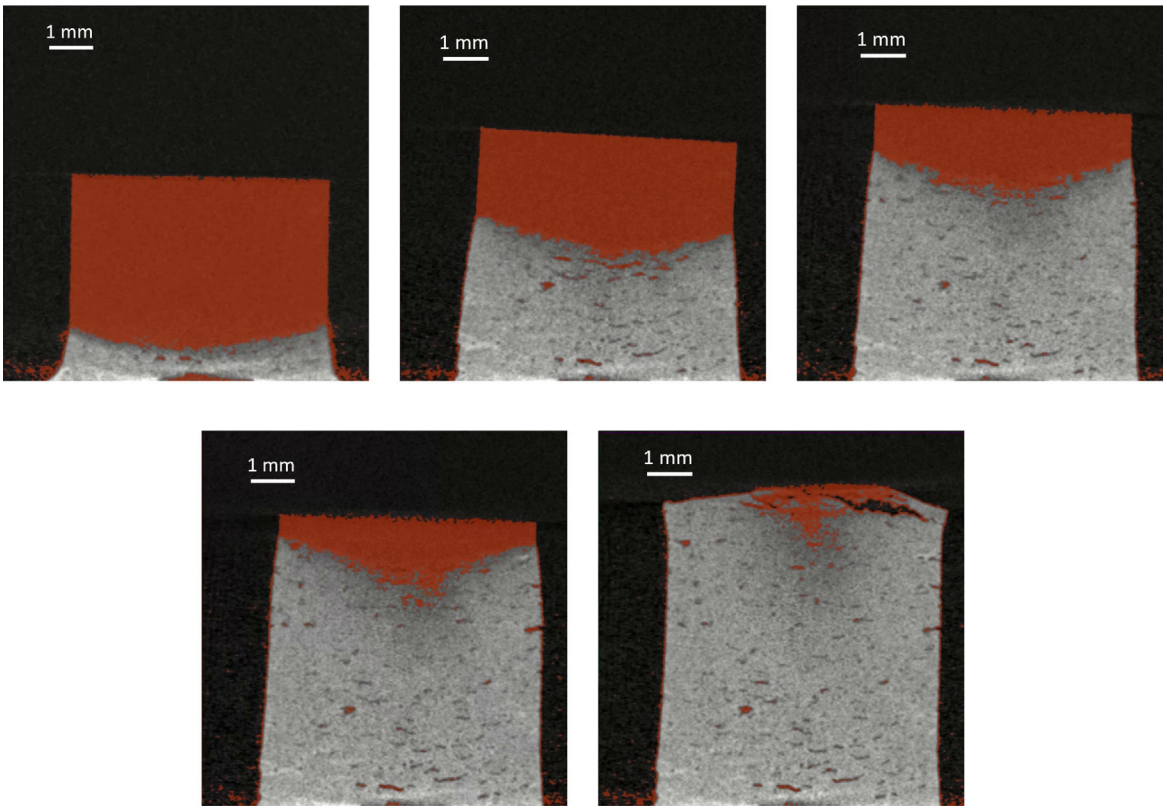

Fig. 12.

Fast water uptake by tablet of relative density 0.95. Orange corresponds to the dry tablet and gray corresponds to wet and swollen tablet. Images show water absorption at timestamps 17.4, 58, 98.6, 133.4 and 211.7 s.

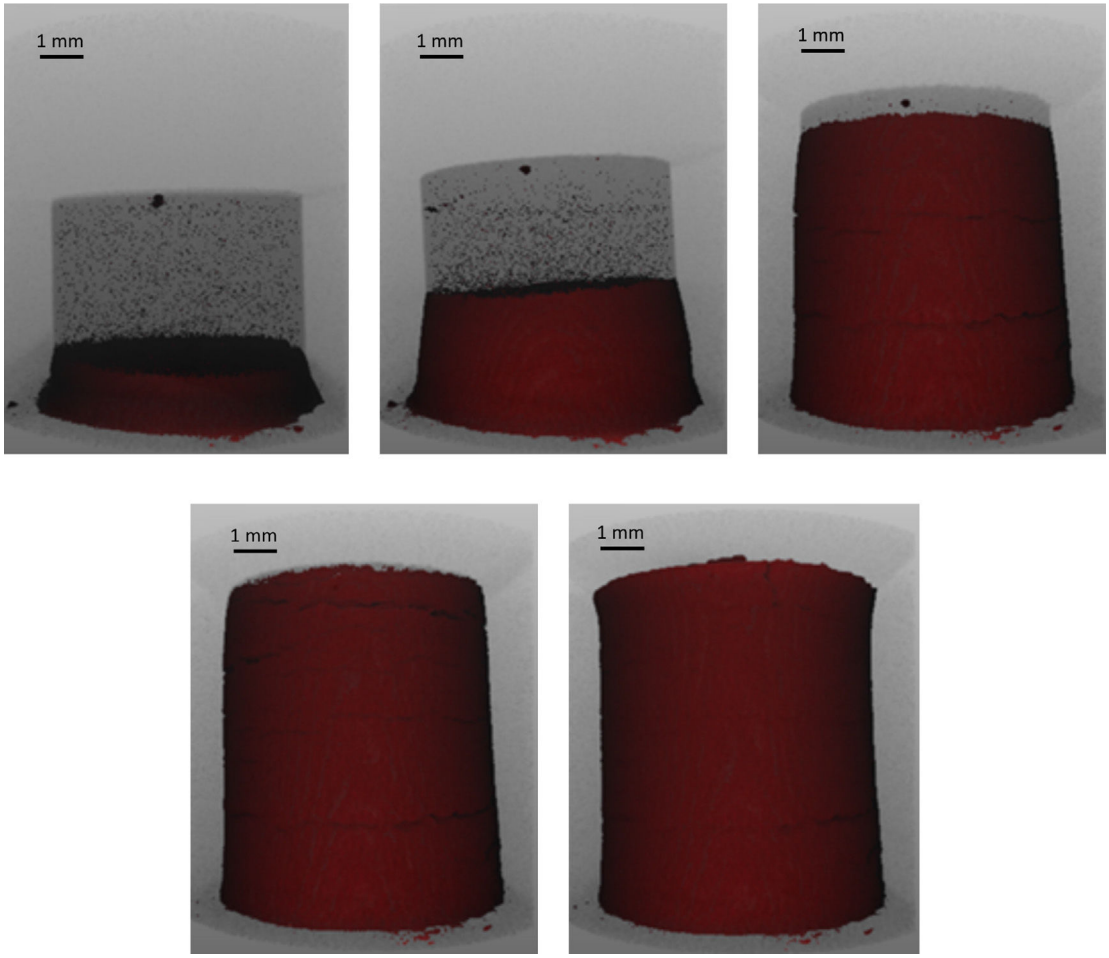

Fig. 13.

Fast water uptake by tablet of relative density 0.95. Dark gray corresponds to the dry tablet and red corresponds to wet and swollen tablet. Images show water absorption at timestamps 14.5, 29, 130.5, 165.3, and 292.9 s.

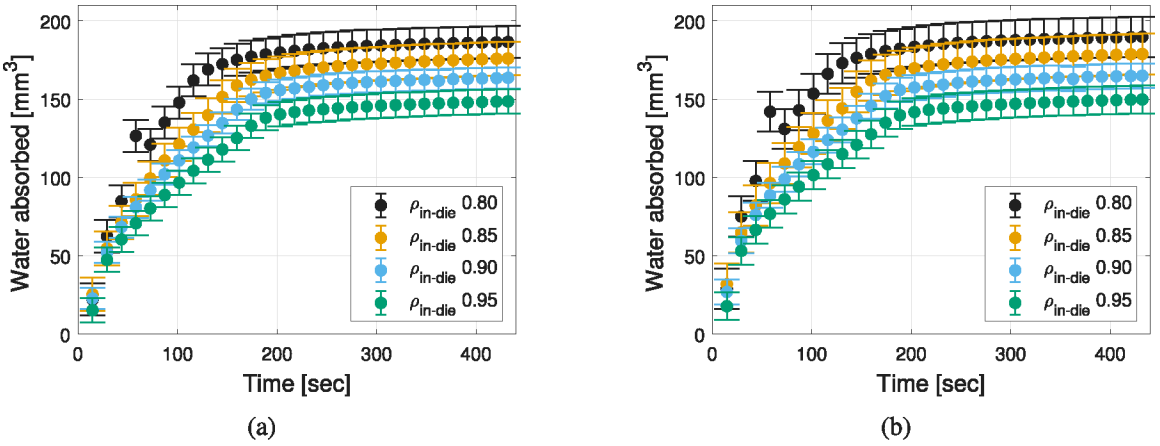

Fig. 14.

Total volume of water absorbed by the tablet. (a) Porosity is assumed fixed during swelling, Eq. (4) is used to generate the results. (b) Porosity is assumed to close during swelling, Eq. (7) is used to generate the results.

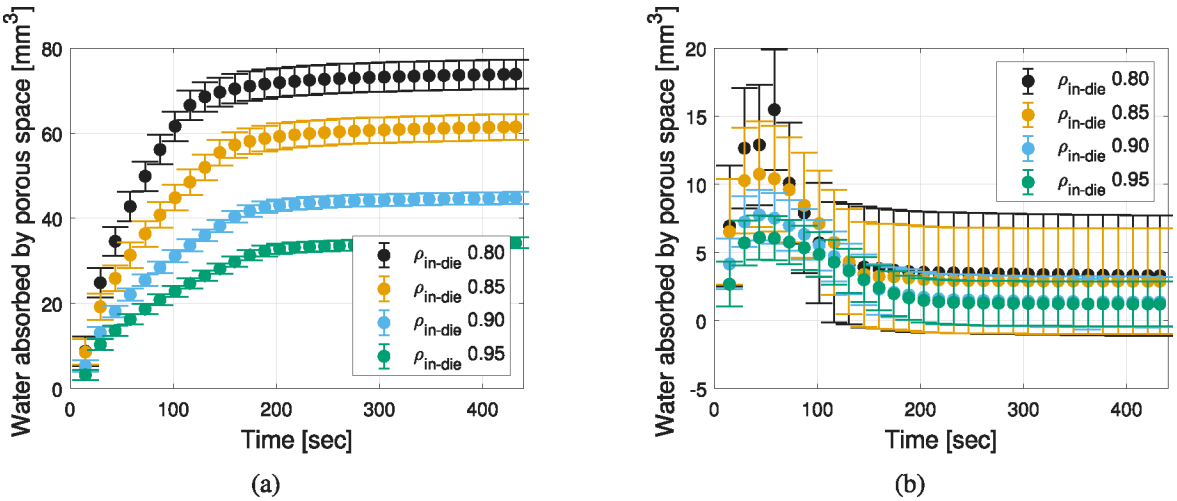

Fig. 15.

Water absorbed by the pore space. (a) Porosity is assumed fixed during swelling, Eq. (3) is used to generate the results. (b) Porosity is assumed to close during swelling, Eq. (9) is used to generate the results.

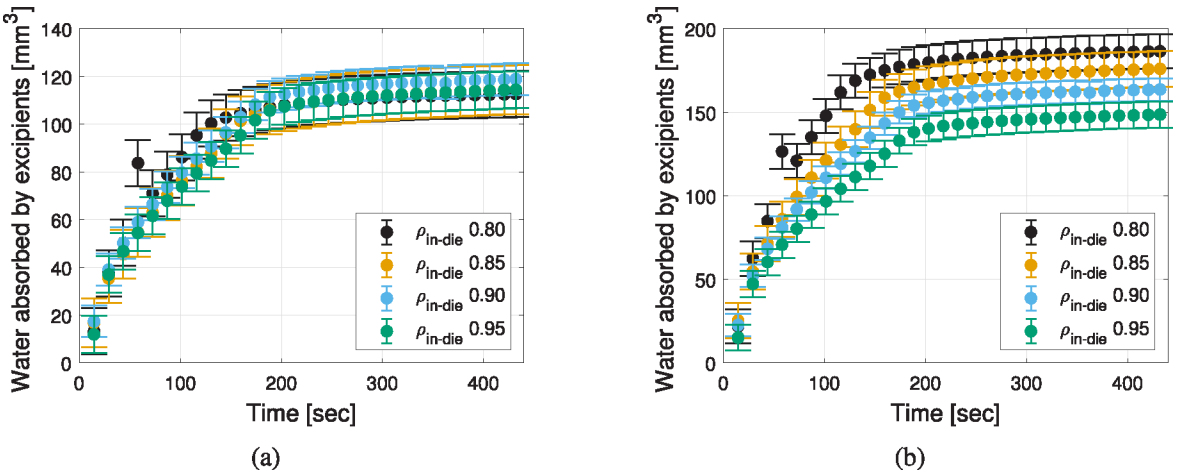

Fig. 16.

Water absorbed by the excipients. (a) Porosity is assumed fixed during swelling, Eq. (2) is used to generate the results. (b) Porosity is assumed to close during swelling, Eq. (8) is used to generate the results.

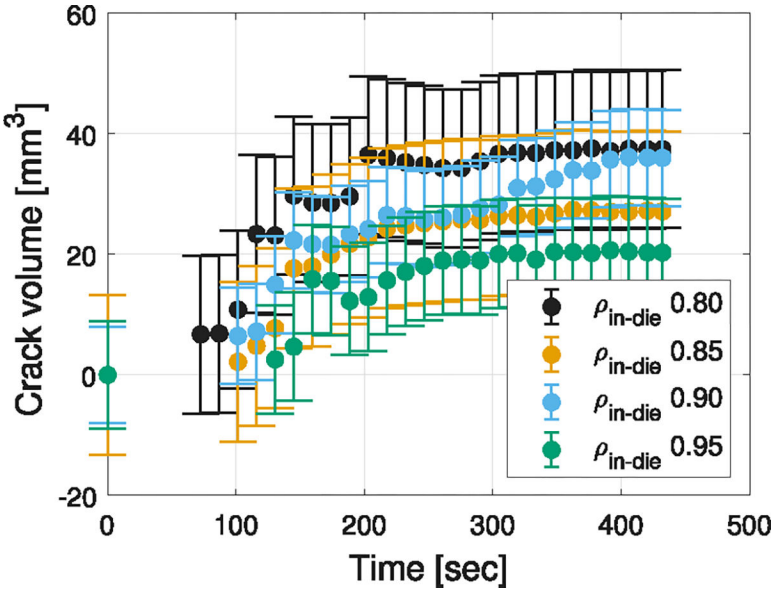

Fig. 17.
Formation of crack inside the tablet over time.

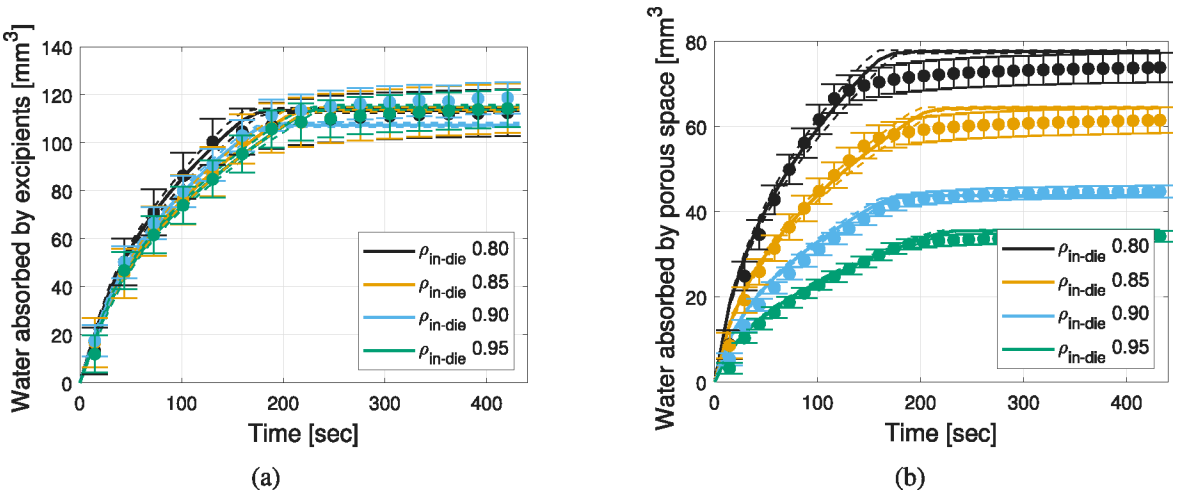

Fig. 18.

Water absorption plots. Circles represent experimental data and lines represent predictions, with dashed curves being the 95% confidence interval of the prediction. (a) Water absorbed by the excipients (using Eq. (12) and experimental data in Fig. 16(a)). (b) Water absorbed by the pore space (using Eq. (13) and experimental data in Fig. 15(a)).

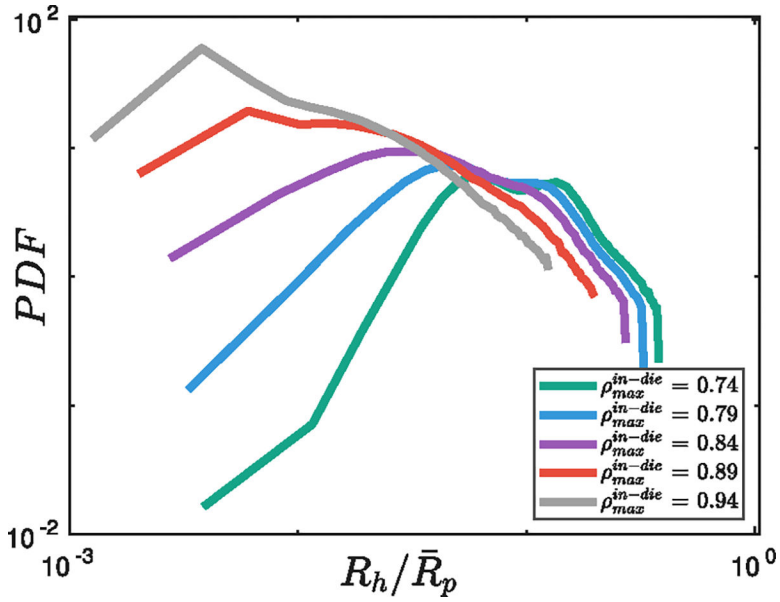

Fig. 19.

Pore-space statistical signature of a die-compacted monodisperse spherical packing at five different relative densities. The hydraulic radius, $R_h = V_t/S_t$, is calculated from figure 11 in Martins and Gonzalez (2022), and $\bar{R}_p$ is the particle radius.

Table 1

Range of attenuation values for tablets of different in-die relative density (ρ_{in-die}).

ρ_{in-die}	**80%**	**85%**	**90%**	**95%**
V_{wet}	21055–64200	18000–54224	17700–47482	21400–61673
V_{total}	16000–64200	14700–54224	14400–47482	16000–61673

Table 2

Properties of the powder blend and the liquid (Markl et al., 2017; Steele et al., 2008). Particle coating and lubrication conditions may affect the contact angle θ (Kristó et al., 2010). Estimated model parameters are reported with 95% confidence intervals.

Property	Unit	Value	Estimation
γ	N/m	72.3×10^{-3}	–
θ		64.3°	–
η	Pa s	1.002×10^{-3}	–
WAC	w/w	–	79.6% ± 0.7%
k	1/s	–	0.10 ± 0.02

Table 3

Estimated effective capillary radius is reported with 95% confidence intervals.

$\rho_{\text{in-die}}$	**Tablet porosity** ϵ_0	**Estimated value of** r_e [nm]
0.80	0.26	10.0 ± 0.8
0.85	0.23	7.3 ± 0.5
0.90	0.17	6.9 ± 0.3
0.95	0.14	5.5 ± 0.3